Bayesian neural network model for austenite formation in steels

L. Gavard, H. K. D. H. Bhadeshia, D. J. C. MacKay, and S. Suzuki

The formation of austenite during the continuous heating of steels was investigated using neural network analysis with a Bayesian framework. An extensive database consisting of the detailed chemical composition, Ac_1 and Ac_3 temperatures, and the heating rate was compiled for this purpose, using data from the published literature. This was assessed using a neural network, with the aim of modelling the austenite start and finish temperatures. The results from the neural network analysis were consistent with what might be expected from phase transformation theory. MST/3373

 Manuscript received 23 May 1995. *Mr Gavard is at the University de Lille I (EUDIL), Lille, France, Dr Bhadeshia and Dr MacKay are in the Mathematics and Physical Sciences Group, Darwin College, University of Cambridge, UK, and Mr Suzuki is with the NKK Corporation, Japan.*

Introduction

Most commercial processes rely to some extent on heat treatments which cause the steel to revert to the austenitic condition. This includes the processes involved in the manufacture of wrought steels, and in the fabrication of steel components by welding. It is useful, therefore, to be able to model quantitatively the transformation of an ambient temperature steel microstructure into austenite.[1]

The formation of austenite during heating differs in many ways from those transformations that occur during the cooling of austenite. For cooling transformations, the kinetics of decomposition follow the classical *C* curve behaviour, in which the rate goes through a maximum as a function of the undercooling below the equilibrium transformation temperature. This is because diffusion becomes sluggish with decreasing temperature, but the driving force for transformation increases with increasing undercooling. Conversely, both the diffusion coefficient and the driving force increase with the extent of superheat above the equilibrium temperature, so that the rate of austenite formation increases indefinitely with temperature (Fig. 1).

There is another important difference between the transformation of austenite, and the transformation to austenite. In the former case, the kinetics of transformation can be described completely in terms of the alloy composition and the austenite grain size. By contrast, the microstructure from which austenite may grow can be infinitely varied. Many more variables are therefore needed to describe the kinetics of austenite formation. The extent to which the starting microstructure has to be specified remains to be determined, but factors such as particle size, the distribution and chemistry of individual phases, homogeneity, the presence of non-metallic inclusions, should all be important.

This discussion highlights the complexity of the problem. A fundamental attempt at modelling the formation of austenite is therefore unlikely to be of general value, except at slow heating rates consistent with the achievement of equilibrium. Some aspects of the difficulties involved have been reviewed recently for a variety of starting microstructures.[2] Models of specific metallurgical approaches exist for austenite formation from a mixture of cementite and ferrite,[3] from bainite,[4] and from ferrite.[5] However, none of these are of general applicability for the reasons described above.

In this work a different approach is adopted involving the use of an artificial neural network to 'blindly' model a large set of published experimental data on austenite formation in steels. The results are then compared extensively against what might be expected on the basis of metallurgical theory.

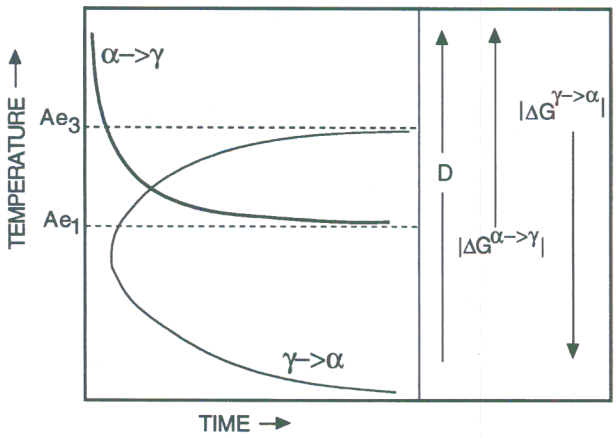

α = ferrite; γ = austenite; ΔG = chemical driving force for transformation; D = rate controlling diffusion coefficient

1 Time–temperature–transformation curves for $\gamma \rightarrow \alpha$ reaction and for reverse $\alpha \rightarrow \gamma$ transformation

Technique

Neural networks are parametrised non-linear models used for empirical regression and classification modelling. Their flexibility enables them to discover more complex relationships between the data than traditional linear statistical models.

A neural network is 'trained' on a set of examples of input and output data. The outcome of the training is a set of coefficients (referred to as weights) and a specification of the functions which in combination with the weights relate the input to the output. The training process involves a search for the optimum non-linear relationship between the input and output data and is computer intensive. Once the network is trained, estimation of the outputs for any given inputs is very rapid.

One of the difficulties with blind data modelling is that of 'overfitting', in which spurious details and noise in the training data are overfitted by the model. This gives rise to solutions that generalise poorly. MacKay[6–11] has developed a Bayesian framework for neural networks in which the appropriate model complexity is inferred from the data.

The Bayesian framework for neural networks has two further advantages. First, the significance of the input variables is automatically quantified. Consequently the

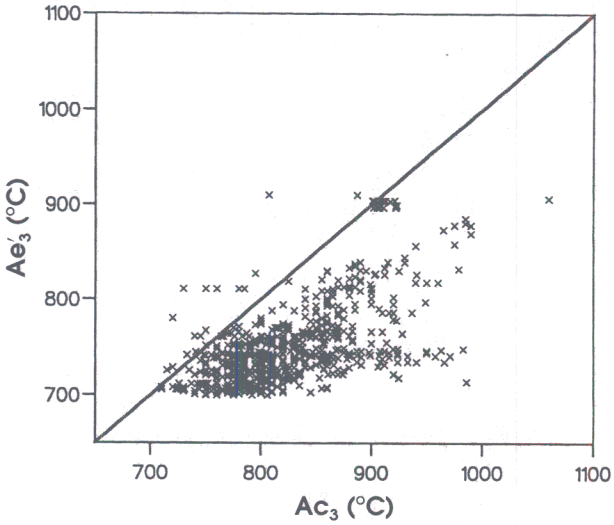

2 Comparison of kinetic Ac_3 temperature with calculated paraequilibrium Ae'_3 temperatures for low alloy steels included in data set

significance perceived by the model of each input variable can be compared against metallurgical theory. Second, the network's predictions are accompanied by error bars which depend on the specific position in input space. These quantify the model's certainty about its predictions.

Database

The data set was constructed using information from the published literature, particularly time–temperature–transformation atlases.[12–16] The variables accessed are listed in Table 1. The data set therefore consisted of 22 input variables, and two output variables, the Ac_1 and Ac_3 temperatures, which respectively describe the onset and completion of austenite formation during continuous heating beginning from ambient temperature. There were 788 cases included in the analysis.

It is expected that the measured Ac_3 temperature would always be higher than the temperature at which the austenite would become fully austenitic under equilibrium conditions (i.e. the Ae_3 temperature). To demonstrate this, the measured Ac_3 temperatures for each of the low alloy steels were compared against the corresponding calculated paraequilibrium Ae'_3 temperatures.* The method for calculation has been described in a previous work.[17] Figure 2 shows that the measured Ac_3 temperatures are almost always larger than the corresponding Ae_3 temperatures, often by several hundred kelvin. Thus, the Ac_3 temperatures in the data set are dominated by kinetic effects and it is therefore important to include the heating rate as a variable.

Table 1 Data set of variables

	Range	Mean	Standard deviation
Concentration, wt-%			
C	0–0·96	0·30	0·17
Si	0–2·13	0·39	0·41
Mn	0–3·06	0·82	0·38
S	0–0·09	0·007	0·011
P	0–0·12	0·008	0·012
Cu	0–2·01	0·046	0·13
Ni	0–9·12	1·01	1·48
Cr	0–17·98	1·23	2·38
Mo	0–4·80	0·32	0·37
Nb	0–0·17	0·003	0·013
V	0–2·45	0·05	0·13
Ti	0–0·18	0·0014	0·014
Al	0–1·26	0·006	0·061
B	0–0·05	0·0005	0·003
W	0–8·59	0·06	0·48
As	0–0·02	0·0001	0·007
Sn	0–0·008	0·0001	0·0003
Zr	0–0·09	0·0001	0·003
Co	0–4·07	0·06	0·42
N	0–0·06	0·003	0·012
O	0–0·005	0·0001	0·0002
Heating rate, K s^{-1}	0·03–50	1·0	11·6
Ac_1, °C	530–921	724	52·2
Ac_3, °C	651–1060	819	55·2

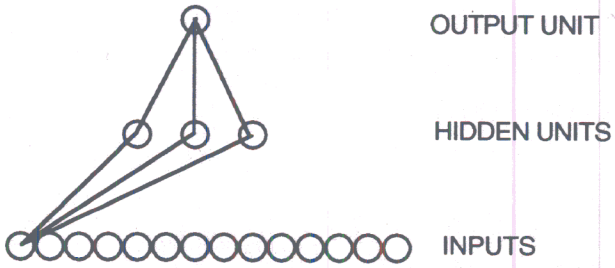

3 Typical network used in analysis: only connections originating from one input unit are shown, the two bias units are not shown

Analysis

The aim of the present work was to predict the austenite formation temperatures for the steels as a function of the variables listed in Table 1. Both the input and output variables were first normalised within the range $\pm 0{\cdot}5$ as follows

$$x_N = \frac{x - x_{min}}{x_{max} - x_{min}} - 0{\cdot}5 \quad \ldots\ldots\ldots\ldots (1)$$

where x_N is the normalised value of x which has maximum and minimum values given by x_{max} and x_{min}, respectively.

The network consisted of 22 input nodes, a number of hidden nodes, and an output node representing either the Ac_1 or the Ac_3 temperature (Fig. 3). The network was trained using 394 of the examples randomly chosen from a total of 788 available, the remaining 394 examples being used as 'new' experiments to test the trained network.

Linear functions of the inputs x_j are operated on by a hyperbolic tangent transfer function

$$h_i = \tanh\left(\sum_j w_{ij}^{(1)} x_j + \theta_i^{(1)}\right) \quad \ldots\ldots\ldots\ldots (2)$$

so that each input contributes to every hidden unit. The bias is designated θ_i and is analogous to the constant that appears in linear regression. The strength of the transfer function is in each case determined by the weight w_{ij}. The transfer to the output y is linear

$$y = \sum_i w_{ij}^{(2)} h_i + \theta^{(2)} \quad \ldots\ldots\ldots\ldots (3)$$

The specification of the network structure together with the set of weights is a complete description of the formula

* The paraequilibrium Ae'_3 temperature is calculated in the same way as the equilibrium Ae_3 temperature, but while maintaining the iron to substitutional solute atom ratio constant everywhere. This means that substitutional solute atoms do not partition between the phases. The paraequilibrium temperature is easier to calculate but always represents an underestimate of the Ae_3 temperature.

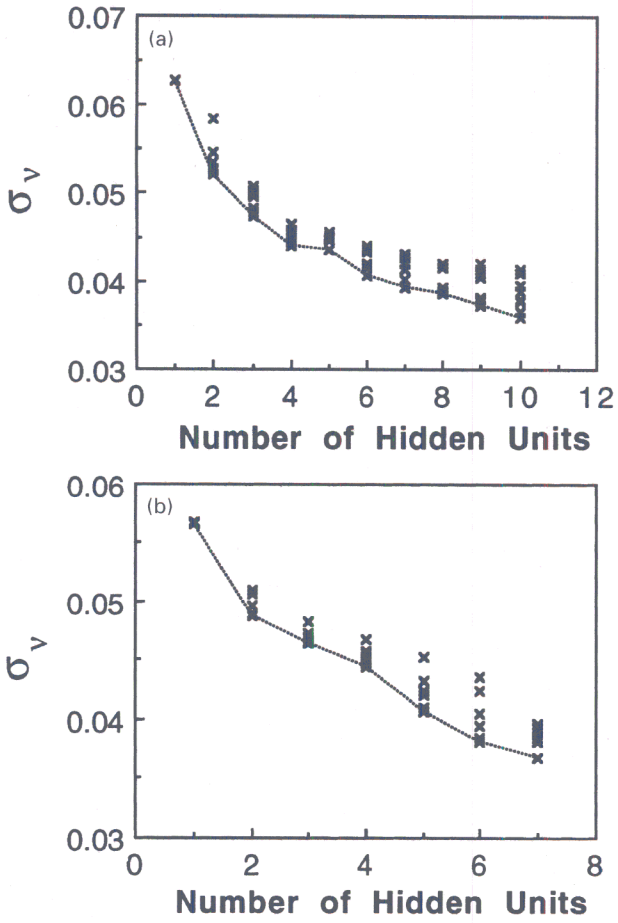

a analysis for Ac_1 temperature; *b* analysis for Ac_3 temperature

4 Variation in framework estimate of noise level of data σ_v as function of number of hidden units: several values are presented for each set of hidden units because training for each network was started with variety of random seeds

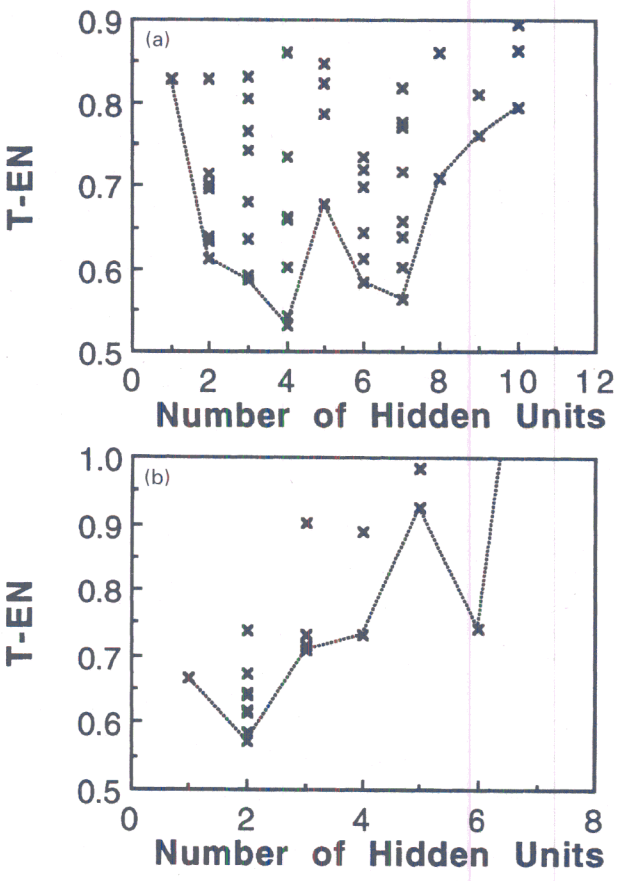

a analysis of Ac_1 data; *b* analysis of Ac_3 data

5 Test error T-EN as function of number of hidden units: several values are presented for each set of hidden units because training for each network was started with variety of random seeds

relating the inputs to the output. The weights are determined by training the network; the details are described elsewhere.[6–8,10,11] The training involves a minimisation of the regularised sum of squared errors. The term σ_v used below is the framework estimate of the noise level of the data.

The complexity of the model is controlled by the number of hidden units (Fig. 4), and the values of the 24 regularisation constants σ_w, one associated with each of the 22 inputs, one for biases, and one for all weights connected to the output.

Figure 4 shows that for both cases, the inferred noise level decreases as the number of hidden units increases. However, the complexity of the model also increases with the number of hidden units. A high degree of complexity may not be justified, and in an extreme case, the model may meaninglessly attempt to fit the noise in the experimental data. MacKay has made a detailed study of this problem and has defined a quantity (the 'evidence') which comments on the probability of a model. In circumstances where two models give similar results over the known data set, the more probable model would be predicted to be that which is simpler; this simple model would have a higher value of evidence. The evidence framework was used to control the regularisation constants and σ_v. The number of hidden units was set by examining the performance on the test data (Fig. 5). A combination of Bayesian and pragmatic statistical techniques was therefore used to control the complexity of the model. Four hidden units were found to give a reasonable level of complexity to represent the variations in the Ac_1 temperature as a function of the input variables. A less complex model (two hidden units) was needed for the Ac_3 temperature, presumably because this should be less dependent on the starting microstructure.

Once the optimum number of hidden units was established for each analysis, the data were retrained to give a more accurate model. This time, all 788 of the cases were included in the training process.

The weights for the selected networks are presented in the Appendix; these listings are sufficient to reproduce the predictions described, though not the error bars. The levels of agreement for the training data sets are shown in Fig. 6, which shows good prediction. It should be emphasised that all data were included in deriving the weights given in the Appendix. It was established that good fit existed over the range of data included in the analysis.

Use of model

The metallurgical significance of the preceding results is now examined. Figure 7 illustrates the significance σ_w of each of the input variables, as perceived by the neural network, in influencing the austenite transformation temperatures, within the limitations of the data set. A high value of σ_w implies that the input parameter concerned explains a relatively large amount of the variation in transformation temperature in the data set (rather like a partial correlation coefficient in multiple regression analysis). It follows that σ_w is not necessarily an indication of the sensitivity of the transformation temperature to that input parameter. The

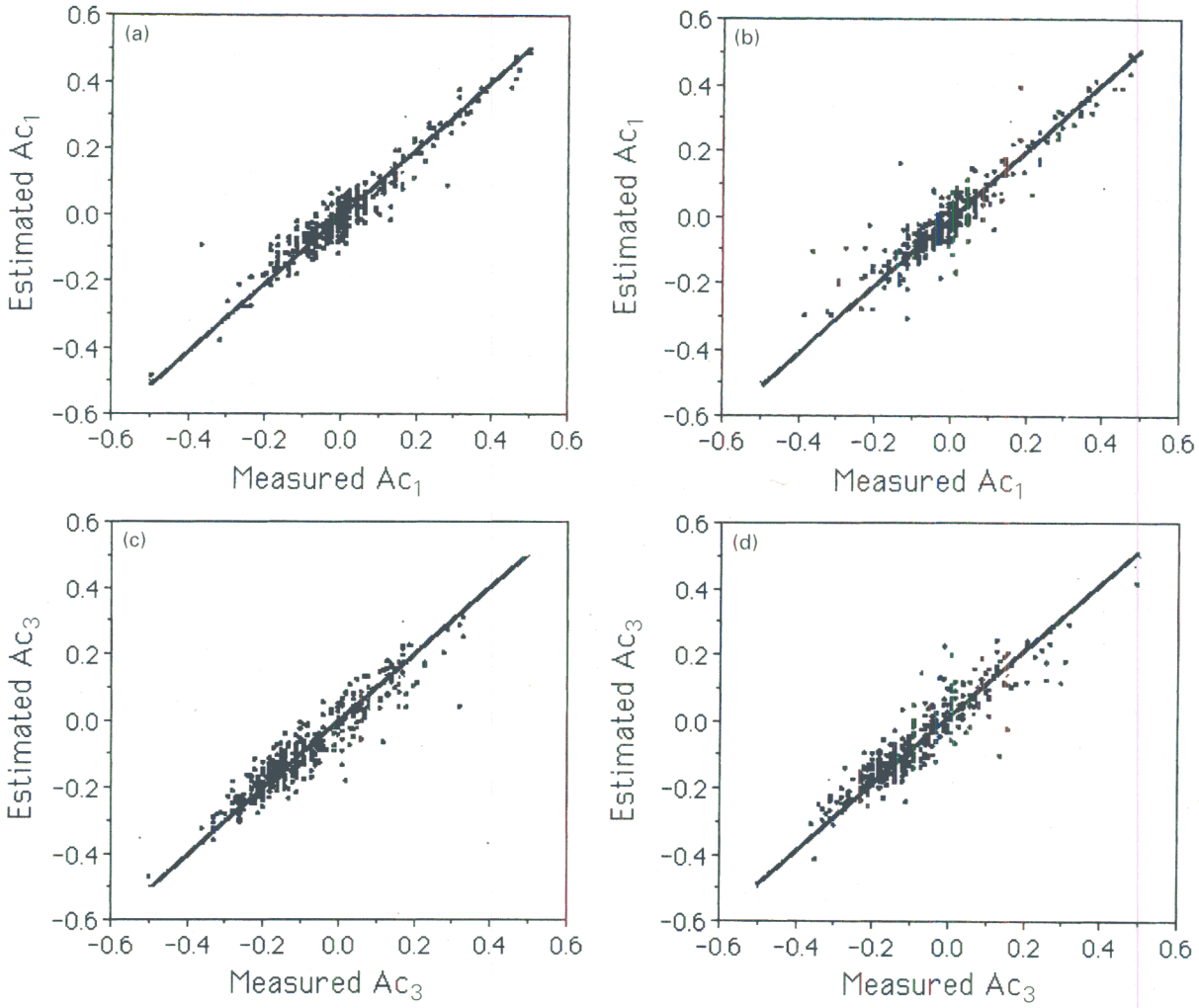

a training data set for Ac_1 temperature, four hidden units used; *b* test data set for Ac_1 temperature, four hidden units used; *c* training data set for Ac_3 temperature, two hidden units used; *d* test set for Ac_3 temperature, two hidden units used

6 Plot of estimated *v.* measured transformation temperatures

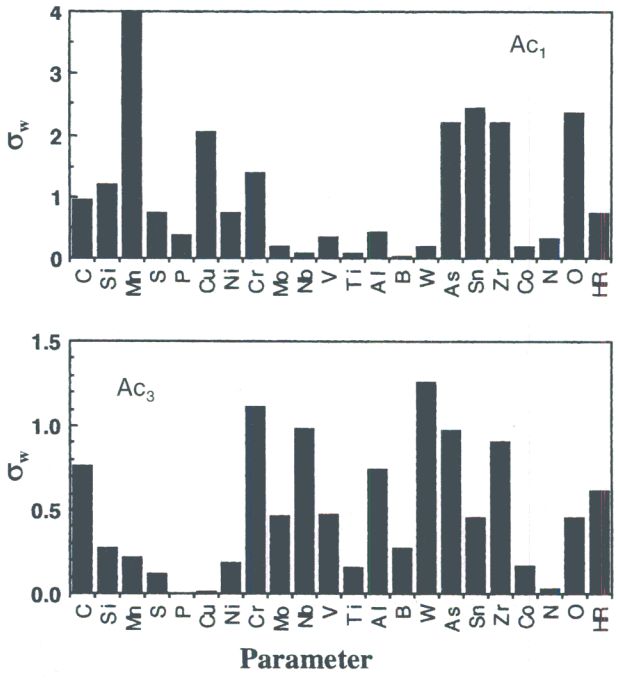

HR = heating rate

7 Histogram showing measure of model perceived significance σ_w of each of input variables in influencing either Ac_1 or Ac_3 temperature

interpretation of σ_w is therefore best considered alongside the predictions of transformation temperatures presented below.

Figure 8 shows the predicted effects of the carbon concentration and heating rate on the Ac_1 and Ac_3 temperatures of a plain carbon steel. The data presented as a function of carbon are calculated for a heating rate of 1 K s^{-1}. As might be expected, the Ac_1 temperature decreases with carbon concentration, reaching a limiting value which is very close to the eutectoid temperature of about 723°C. This limit is expected because of the slow heating rate and the fact that the test steel does not contain any substitutional solutes. Note that there is a slight underprediction of the Ac_1 temperature for pure iron, although the expected temperature of about 910°C is within the 95% confidence limits of the prediction (twice the width of the error limits illustrated in Fig. 8).

By contrast, the Ac_3 temperature appears to go through a minimum at about the eutectoid carbon concentration. This is also expected because the Ae_3 temperature also goes through a minimum at the eutectoid composition. Furthermore, unlike the Ac_1 temperature, the minimum value of the calculated Ac_3 never reaches the eutectoid temperature; even at the slow heating rate it is expected that the austenite transformation finishes at some superheat above the eutectoid temperature, the superheat being reasonably predicted to be about 25 K.

At slow heating rates, the predicted Ac_1 and Ac_3 temperatures are in fact very close to the equilibrium Ae_1

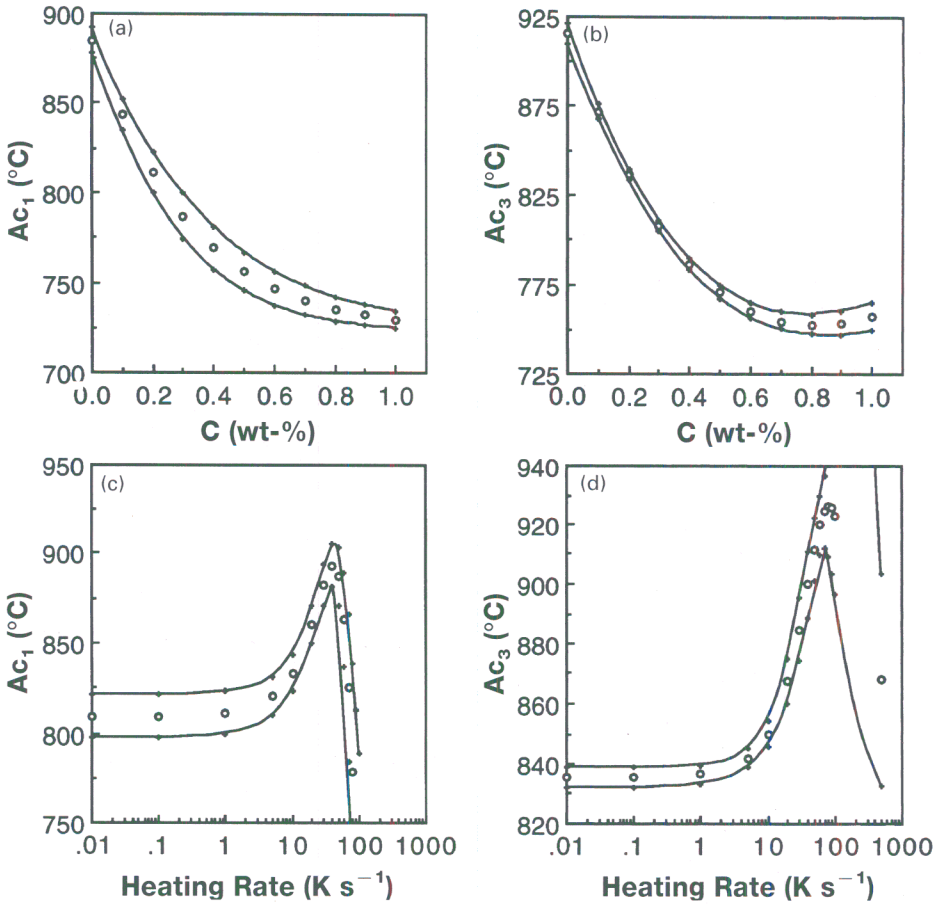

a predicted variation in Ac_1 as function of carbon concentration of plain carbon steel, heating rate of 1 K s^{-1}; four hidden units used; *b* predicted variation in Ac_3 as function of carbon concentration of plain carbon steel, heating rate of 1 K s^{-1}; two hidden units used; *c* predicted variation in Ac_1 temperature of Fe–0·2C (wt-%) alloy as function of heating rate, four hidden units used; *d* predicted variation in Ac_3 temperature of Fe–0·2C (wt-%) alloy as function of heating rate, two hidden units used

8 Predicted variation in Ac_1 and Ac_3 temperatures: lines represent $\pm 1\sigma$ error bars about calculated points

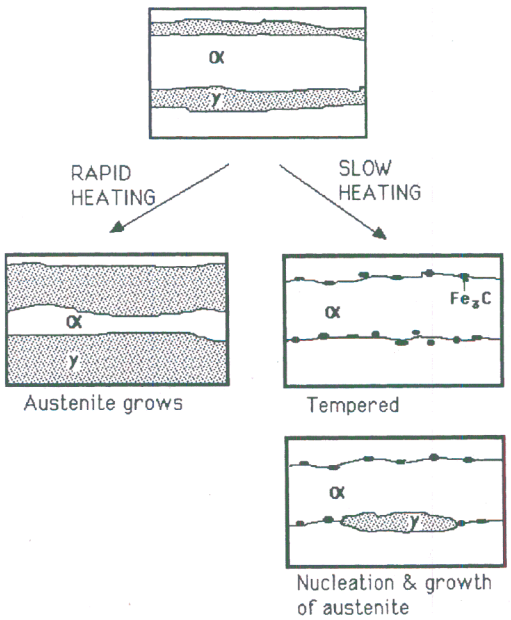

9 Schematic diagram illustrating why when critical heating rate is exceeded, smaller superheat is necessary to grow austenite: very large heating rate can involve growth of existing retained austenite, thereby avoiding need to nucleate new austenite, hence leading to decrease in superheat needed to begin transformation[4]

and Ae_3 temperatures and insensitive to the rate of heating. As expected, they both increase more rapidly when the heating rate exceeds about 10 K s^{-1}. Since the mean heating rate in the experimental data set is only 1 K s^{-1} (Table 1), it is not surprising that the σ_w values associated with the heating rate are relatively small in Fig. 7.

It is not at first sight expected that the transformation temperatures would go through a maximum as a function of the heating rate. This maximum appears to be significant even when the error bars are taken into account. It should be noted that the predicted errors become very large at heating rates well outside the range of the experimental database. The occurrence of a maximum is possible if retained austenite is present in the microstructure, as might be the case for many of the steels for which high heating rate experiments have been conducted. This is because at high heating rates, the retained austenite simply grows as soon as the equilibrium Ae_1 temperature is exceeded. However, slow heating allows the austenite to first decompose into an equilibrium mixture of ferrite and carbides, thereby making it necessary for new austenite to nucleate when equilibrium permits. This is shown in Fig. 9.

Figure 7 shows that the σ_w value for manganese is larger for the Ac_1 data than for the corresponding Ac_3 data. Noting also that the variation of manganese in the data set is large, and that the data are likely to be reliable since it is a key alloying element in steel, it is likely that the difference in the two σ_w values is important. This is confirmed by the predicted effect of manganese on the transformation temperatures (Fig. 10*a*), since the Ac_1

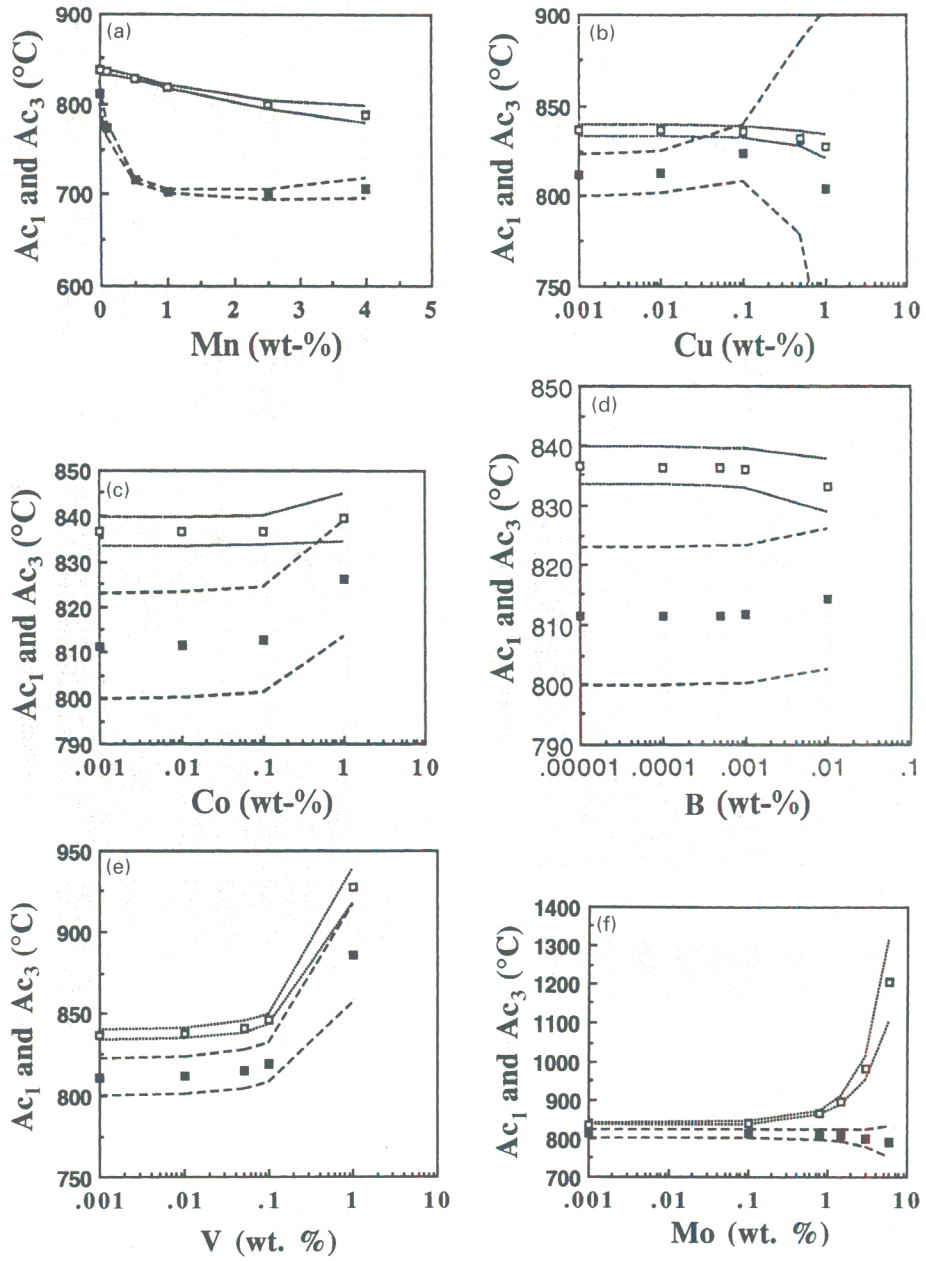

a manganese; *b* copper; *c* cobalt; *d* boron; *e* vanadium; *f* molybdenum

10 Predicted variation in Ac_1 and Ac_3 temperatures as function of concentration of given alloying elements for Fe–0·2C (wt-%) steels at heating rate of 1 K s^{-1}: lines represent $\pm$ 1σ error bars about calculated points

temperature is indeed found to be more sensitive to manganese than the Ac_3 temperature. This behaviour is also expected from the Fe–C–Mn phase diagram. Whereas the effect of manganese on the Ac_3 temperature is simply to lower the $(\alpha+\gamma)/\gamma$ phase boundary on the temperature scale (via the thermodynamic effect of manganese on austenite stability), the influence on Ac_1 is much larger since a three phase $\alpha+\gamma+M_3C$ field develops. This is confirmed by the phase diagram calculations carried out using the MTDATA (1995) thermodynamic package.[18] Thus, the Ae_1 and Ae_3 temperatures for Fe–0·2C–1Mn (unless otherwise stated all compositions given in this paper are in weight per cent) alloy were predicted to be 696 and 823°C, respectively. This compares with the corresponding equilibrium temperatures for a plain carbon Fe–0·2C steel of 723 and 839°C. Thus, manganese should indeed influence Ac_1 more than Ac_3 in the present context. The calculations allowed for the existence of ferrite, austenite, and M_3C, where M refers to metal atoms.

Figure 10*b* shows that copper, over the concentration range considered, has a negligible influence on the formation of austenite. The difference between the Ac_1 and Ac_3 temperatures decreases with increasing cobalt concentration (Fig. 10*c*).

Boron has consistently small values of σ_w for both the Ac_1 and Ac_3 temperatures (Fig. 7). Table 1 shows that there is a significant concentration range of boron included in the data set, the maximum boron content being 500 ppm by weight. The concentration of boron can be precisely controlled in steel to an accuracy of $\pm$5 ppm by weight, and the accuracy of the chemical analysis is generally better than $\pm$3. Consequently a low value of σ_w truly indicates that the austenite formation temperatures are insensitive to the boron concentration, and this is confirmed by the predicted effect of boron in Fig. 10*d*.

Vanadium is an extremely strong carbide forming element, with limited solubility even in austenite. Hence, it is not surprising that both the Ac_1 and Ac_3 temperatures

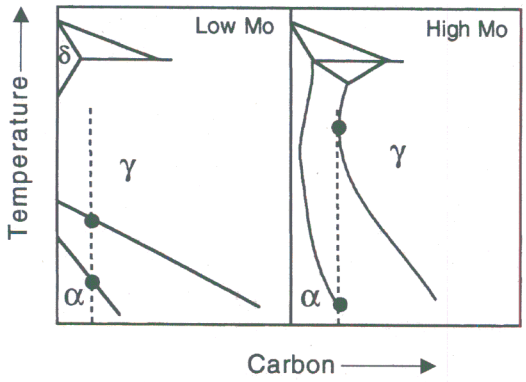

11 Schematic diagram illustrating way molybdenum modifies phase diagram of steel: at low concentrations, the α and δ ferrite phase fields are separated but they connect when the molybdenum concentration is increased which leads to large change in Ac_3 temperature though not in the Ac_1 temperature, as indicated by pairs of points marked on each diagram

are very high for the Fe–0·2C–1V alloy. Austenite growth is retarded if the carbon is tied up in the form of vanadium carbide.

When compared with vanadium, molybdenum is a less potent carbide forming element. Hence, at comparable concentrations, the transformation temperatures are found to be less sensitive to the molybdenum content. However, at very large molybdenum contents the Ac_3–Ac_1 gap increases greatly. This is because the high temperature δ ferrite and low temperature α ferrite phase fields tend to join up in the low carbon end of the phase diagram, thereby raising the temperature at which austenite formation is completed (Fig. 11). These results are verified by the phase diagram calculations presented in Table 2.

Predicted data for the effects of nickel and chromium are illustrated in Fig. 12. Nickel is an austenite stabiliser, and judging from the phase diagram both the Ac_1 and Ac_3 temperatures should decrease with increasing nickel concentration. This clearly is not the case with the predicted Ac_1 temperature, which seems to exceed the predicted Ac_3 temperature for nickel concentrations greater than about 1% (although the data beyond about 6% are not reliable,

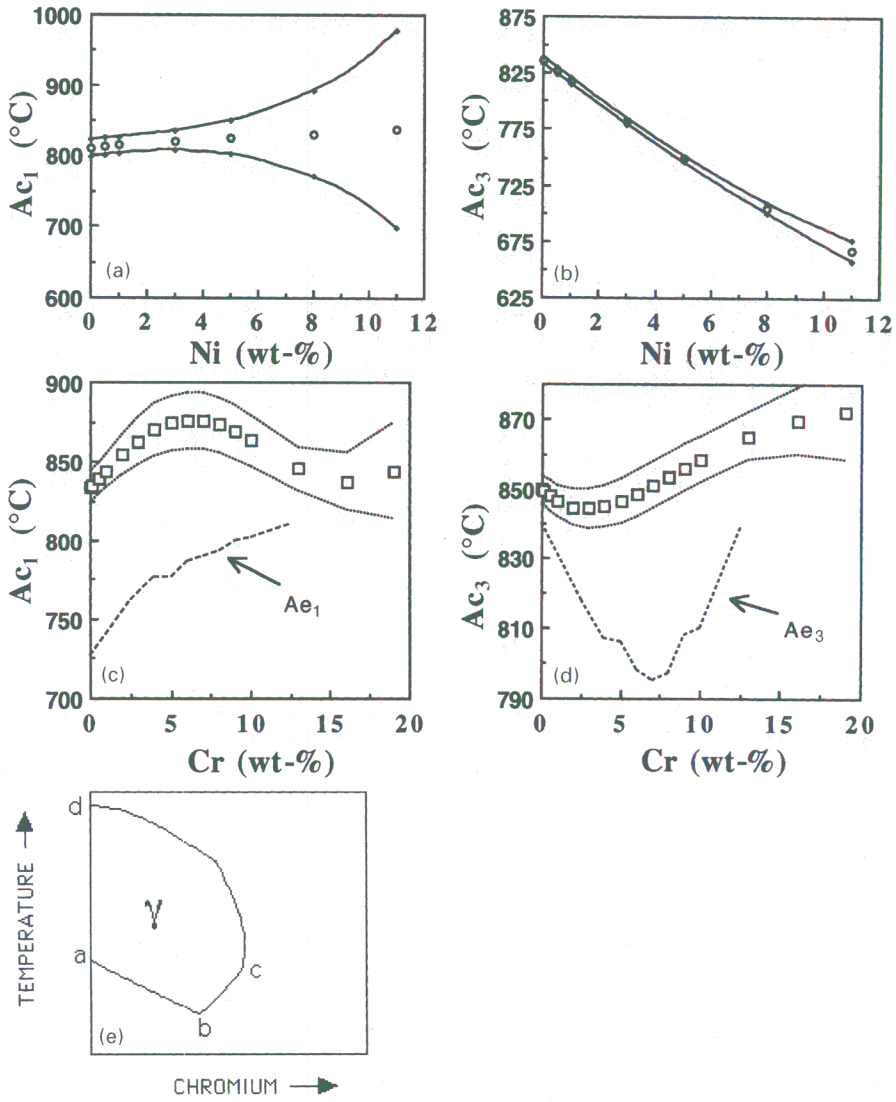

a predicted variation of Ac_1 temperature with nickel concentration; *b* predicted variation of Ac_3 temperature with nickel concentration; *c* predicted variation of Ac_1 temperature with chromium concentration; *d* predicted variation of Ac_3 temperature with chromium concentration; *e* illustration of γ loop, portions *ab*, *bc*, and *cd* represent $(\alpha+\gamma)/\gamma$, $(\gamma+M_{23}C_6)/\gamma$, and $\gamma/(\gamma+\alpha)$ phase boundaries, respectively

12 Predicted variation in Ac_1 and Ac_3 temperatures of Fe–0·2C (wt-%) steel as function of concentration of given alloying element at heating rate of 1 K s^{-1}: lines represent $\pm1\sigma$ error bars about calculated points; effect of chromium on γ loop is also shown

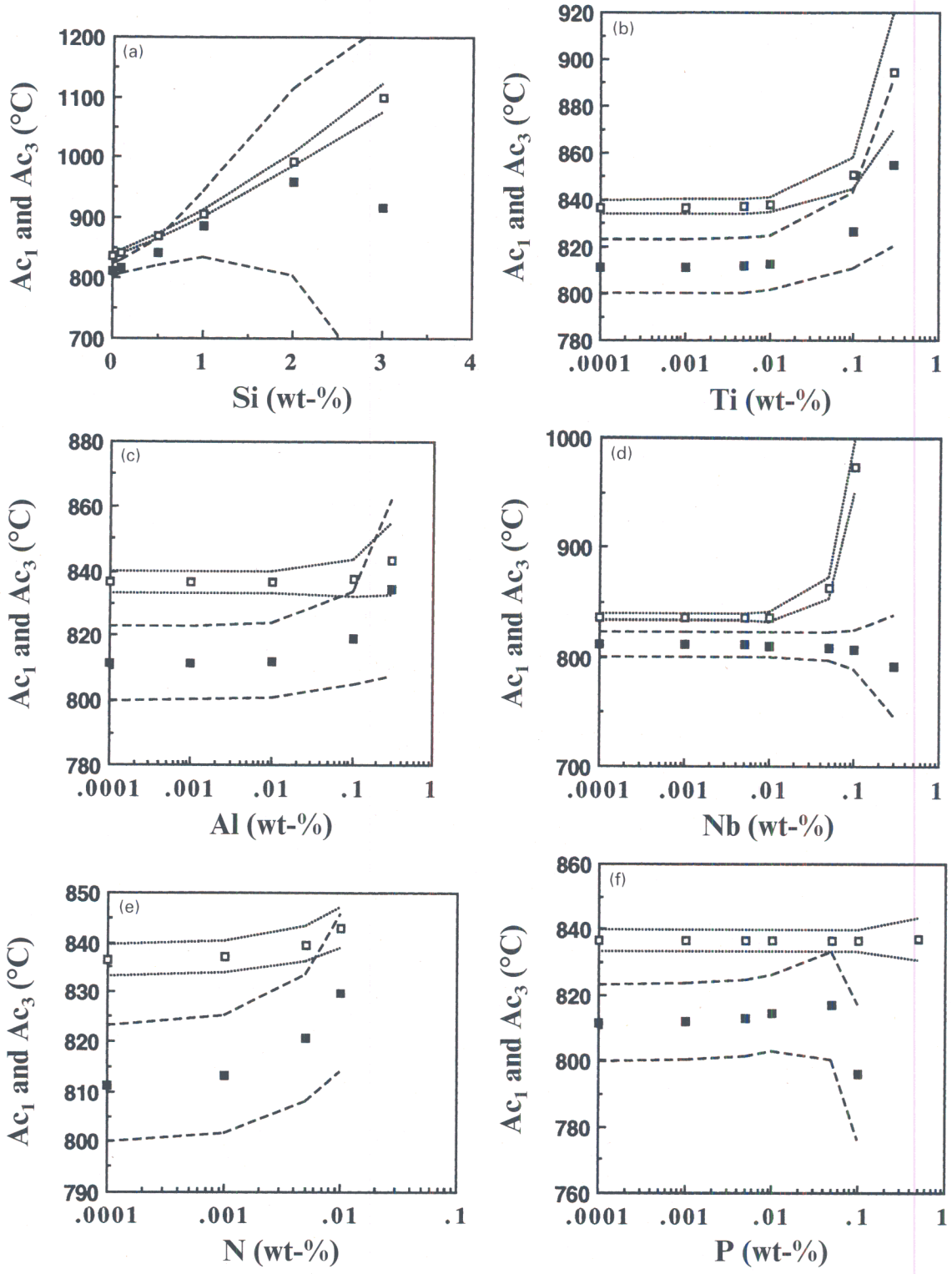

a silicon; *b* titanium; *c* aluminium; *d* niobium; *e* nitrogen; *f* phosphorus

13 Predicted variation in Ac_1 and Ac_3 temperatures of Fe–0·2C (wt-%) steel as function of concentration of given alloying element at heating rate of 1 K s^{-1}: lines represent $\pm 1\sigma$ error bars about calculated points

with large error bars). This behaviour reflects the poor quality of the Ac_1 data for the nickel steels.

The predicted data for chromium are more interesting. The Ac_3 temperature appears to go through a minimum with increasing chromium concentration, a behaviour which is replicated to some extent by the calculated Ae_3 temperatures for the same alloy system. The trend for Ac_1 is different, but follows what is expected from the calculated phase diagram. At about Fe–0·2C–7·5Cr, the Ae_1 temperature becomes virtually identical to the Ae_3 temperature. This is because of the existence of a γ loop in the phase diagram, as shown schematically in Fig. 12*e*. The results for chromium are therefore consistent with what is expected from the phase diagram: there are some results where the calculated Ac_1 exceeds Ac_3, but this is not significant when the error bars are taken into account. The work emphasises that there will be difficulties at high chromium concentrations since the difference between

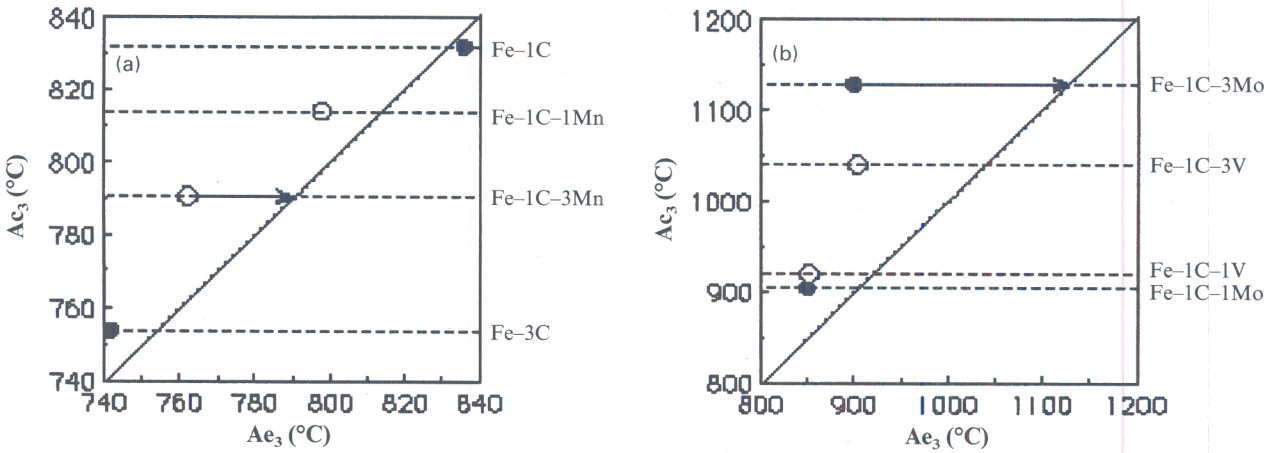

14 Comparison of calculated Ac_3 temperatures with calculated equilibrium Ae_3 temperature: solute concentrations are in atomic per cent, horizontal arrows indicate largest deviation of Ac_3 from Ae_3 in each case

the two transformation temperatures becomes rather small.

Disregarding the effect of silicon on the Ac_1 temperature (due to the unreliability of the predictions with large error bars), its influence on the Ac_3 temperature is consistent with the fact that it is a ferrite stabilising element (Fig. 13). Titanium raises the transformation temperatures, presumably because it is combined with carbon in the initial microstructure. The effect of niobium is similar to that of molybdenum. Nitrogen and phosphorus, at the concentrations studied, have no significant effects on austenite formation, consistent with their small σ_w values (Fig. 7).

Further tests of model

Substitutional solutes affect transformations in steels by two mechanisms:

(i) a solute can alter the relative thermodynamic stabilities of the parent and product phases, e.g. solutes like nickel which stabilise austenite might be expected to lower the Ae_3 temperature, which is an equilibrium transformation temperature

(ii) the solute is likely to have different solubilities in the parent and product phases. When transformation is diffusion controlled, the necessity for the solute to partition is expected to reduce the rate of transformation. This kinetic effect is independent of the thermodynamic effect emphasised in (i).

It is possible, using the trained neural network model, to examine both of these issues, and hence test whether the model behaves correctly from a metallurgical point of view. Figure 14 contains comparisons between the kinetic Ac_3 temperatures and corresponding thermodynamically calculated Ae_3 equilibrium transformation temperatures. Any difference between these represents some kinetic hindrance to transformation.

Figure 14*a* shows clearly that the Fe–C alloys transform easily to austenite, at temperatures which are not very different from equilibrium. The superheat needed for the higher carbon Fe–C alloy is larger because the extra carbon depresses the transformation temperature, leading to a reduction in the mobility of iron atoms. The addition of manganese clearly leads to much larger deviations from equilibrium, even when the transformation occurs at temperatures higher than for the Fe–3C (at.-%) steel. Furthermore, the deviation increases disproportionately with the concentration of manganese. This confirms the fact that the presence of a substitutional solute greatly retards the transformation to austenite because it is necessary for the solute to diffuse during transformation.

To show that it is the diffusion of solute which retards the formation of austenite, Fig. 14*b* shows cases where the

Table 2 Phase equilibrium calculations conducted for a series of Fe–0·2C–Mo (wt-%) alloys using MTDATA (1995)[17]

Alloy composition, wt-%	Ae_1, °C	Ae_3, °C
Fe–0·2C–1Mo	727	845
Fe–0·2C–4Mo	727	897
Fe–0·2C–6Mo	715	955

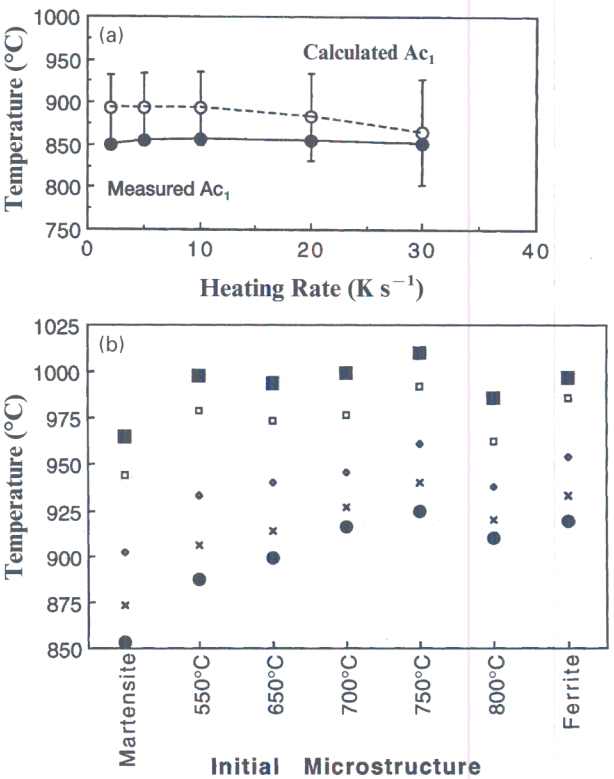

a variation in calculated and measured Ac_1 temperatures; measured temperatures refer to samples with untempered martensitic microstructure; *b* illustration of variation in austenitisation behaviour as function of initial microstructure, tempering time = 1 h: ● Ac_1, ■ Ac_3, × $Ac10\%$, ◆ $Ac50\%$, □ $Ac90\%$

15 Calculations for steel T91: heating rate of 50 K s^{-1} used to measure Ac_1 and Ac_3 temperatures

addition of molybdenum or vanadium raises the transformation temperature, but nevertheless increases the deviation from equilibrium.

Application to steel T91

Steel T91 is an alloy of chemical composition (wt-%) Fe–0·105C–0·43Si–0·37Mn–8·2Cr–0·97Mo–0·13Ni–0·051N –0·075Nb–0·2V which was designed for power plant applications and for use in the nuclear industry. It is of particular interest to the present authors and a number of experiments have been conducted to measure the austenite formation temperatures as a function of the initial microstructure.[19] The initial microstructure has not been included as a variable in the neural network model, because of the absence of data. The following results therefore illustrate the level of error in prediction, which can be attributed to microstructural effects.

Martensite was obtained by directly quenching the alloy after austenitising at 1050°C for 30 min, to room temperature. A number of tempered martensite microstructures were also generated from the quenched samples. In addition, microstructure consisting of allotriomorphic ferrite and alloy carbides of pearlitic appearance was obtained by isothermal transformation of austenite at 725°C for 6 h before cooling to ambient temperature.

The calculated Ac_1 temperature is compared with the value measured for the untempered martensite, as a function of the heating rate, in Fig. 15*a*. The calculation overestimates the transformation temperature by 15–50 K, which is within the error limits of the neural network model. Consistent with the experimental data, the model predicts that the transformation temperature does not increase with the heating rate. If anything, there is a slight decrease predicted.

Figure 15*b* shows the variation in transformation temperatures with the starting microstructure. It is evident that the variation can be as large as 75 K, a value comparable with the overall error implied by the σ_v noise for the optimised neural network models (Fig. 4).

Conclusions

The temperature at which austenite first begins to form during heating, and that at which the transformation to austenite is completed, have been modelled as a function of the steel chemical composition and heating rate. The model is based on a neural network analysis of an experimental database compiled from published data.

The model is found to be capable of estimating the transformation temperatures to an accuracy of about ±40 K (95% confidence limits). The neural network technique used is based on a Bayesian framework and hence is capable of associating different error bars depending on the location in the input parameter space. This has demonstrated that the predictability of the Ac_1 temperature is in many cases less reliable than that of the Ac_3 temperature. This is probably a reflection of the fact that in many cases the Ac_1 temperature is more difficult to measure experimentally. The predictions of the model have been assessed against metallurgical theory and found to be reliable.

Acknowledgements

The authors are grateful to EUDIL (University de Lille I) and Professor Rolland Taillard for facilitating one of the author's (LG) work in Cambridge, and to Professor Colin Humphreys of Cambridge University for his support and encouragement of the work. The authors sincerely thank Machiko Suzuki for her help in transforming some of the data into a computer format.

References

1. H. K. D. H. BHADESHIA and L.-E. SVENSSON: in 'Mathematical modelling of weld phenomena', (ed. H. Cerjak and K. E. Easterling), 109–182; 1993, London, The Institute of Materials.
2. H. K. D. H. BHADESHIA: 'Bainite in steels'; 1992, London, The Institute of Materials.
3. M. HILLERT, K. NILSSON, and L.-E. TORNDAHL: *J. Iron Steel Inst.*, 1971, **209**, 49–66.
4. J. R. YANG and H. K. D. H. BHADESHIA: *Mater. Sci. Eng. A*, 1989, **A118**, 155–170.
5. C. ATKINSON, T. AKBAY, and R. C. REED: *Acta Metall. Mater.*, 1995, **43**, 2013–2031.
6. D. J. C. MacKAY: *Neural Comput.*, 1992, **4**, 415.
7. D. J. C. MacKAY: *Neural Comput.*, 1992, **4**, 448.
8. D. J. C. MacKAY: *Darwin College J.*, March 1993, 81.
9. D. J. C. MacKAY: *ASHRAE Trans.*, 1994, **100**, (2), 1053–1062.
10. D. J. C. MacKAY: *Network*, 1995, **6**, 469–505.
11. H. K. D. H. BHADESHIA, D. J. C. MacKAY, and L.-E. SVENSSON: *Mater. Sci. Technol.*, 1995, **11**, 1046–1051.
12. K. ABIKO: *Sci. Am.*, Japanese edition, January 1993, 20–29.
13. T. COOL: 'Systematic design of welding alloys for power plant steels', CPGS thesis, University of Cambridge, 1994.
14. R. REED: PhD thesis, University of Cambridge, 1987.
15. 'Atlas of isothermal transformation diagrams of BS En steels', 2nd edn; 1956, London, The Iron and Steel Institute.
16. 'Atlas of time–temperature–transformation diagrams for irons and steels', (ed. G. F. Vander Vroot); 1991, Materials Park, OH, ASM International.
17. H. K. D. H. BHADESHIA: *Met. Sci.*, 1982, **16**, 159–165.
18. 'MTDATA, Metallurgical thermochemical data', National Physical Laboratory, Teddington, Middlesex, UK, 1995.
19. J. BRACHET, R. PRADELLES, and L. GAVARD: unpublished research, CEA, Saclay, France, 1995.

Appendix

Table 3 Weights for Ac_1 model*

−0·273272	−0·584284	1·42725	−0·675013	−0·297617	0·149305	−2·09248	0·558102
1·16302	0·136662	0·00893805	0·0271082	0·0482528	0·285341	0·0135071	0·0350339
−0·074152	−0·0884704	−0·0661309	−0·133209	−0·224594	−0·102685	0·810902	−3·00552
−1·58987	0·515423	−7·77932	−1·22046	−0·294707	−0·160822	0·844392	−1·54547
−0·0628648	0·0217054	0·138556	0·0306007	0·124344	0·00430856	0·00473683	1·56578
1·85985	1·57345	0·221986	0·179021	1·77703	−0·646938	0·902249	0·677717
−1·55427	0·638917	0·424401	0·232198	3·09303	−0·533354	0·0072862	−0·120021
−0·0700783	0·415026	0·0173118	−0·0489667	0·00607633	−0·196499	−0·476342	−0·658654
−0·475611	0·177044	0·44253	−0·574891	−0·266723	−0·512698	0·303814	−0·779683
0·417492	0·0995294	−0·542185	0·66351	−0·846634	−1·68699	−0·146489	0·0761116
−0·270882	−0·0883608	−0·413762	$4{\cdot}99285 \times 10^{-6}$	0·162749	0·215546	0·238404	0·221876
0·0765538	0·0192461	0·227757	−0·918695	0·416309	2·72348	1·33381	1·82862
1·8775							

* Data are arranged in a continuous horizontal sequence in the following order:

$\theta_1^{(1)}, w_{1,1}^{(1)} \ldots w_{1,22}^{(1)}$

$\theta_2^{(1)}, w_{2,1}^{(1)} \ldots w_{2,22}^{(1)}$

$\theta_3^{(1)}, w_{3,1}^{(1)} \ldots w_{3,22}^{(1)}$

$\theta_4^{(1)}, w_{4,1}^{(1)} \ldots w_{1,22}^{(1)}$

$\theta^{(2)}, w_1^{(2)} \ldots w_4^{(2)}$.

Table 4 Weights for Ac_3 model*

−1·41522	−0·811777	0·292749	−0·212523	−0·086742	$6{\cdot}22651 \times 10^{-5}$	−0·0097287	−0·224123
−1·03976	0·466825	0·849595	−0·250228	0·123227	−0·56492	0·215049	−0·938616
0·309341	0·0687889	0·255502	−0·129074	0·0229901	0·069863	−0·479553	1·13112
0·70752	−0·241007	0·203091	0·129634	$5{\cdot}8642 \times 10^{-5}$	−0·00661998	0·103754	1·16011
−0·422398	−1·07388	0·545212	−0·131634	0·711098	−0·287479	1·46768	−0·639086
−0·142399	−0·532336	0·171956	0·0100161	−0·143582	0·661583	1·62705	4·13134
2·53442							

* Data are arranged in a continuous horizontal sequence in the following order:

$\theta_1^{(1)}, w_{1,1}^{(1)} \ldots w_{1,22}^{(1)}$

$\theta_2^{(1)}, w_{2,1}^{(1)} \ldots w_{2,22}^{(1)}$

$\theta^{(2)}, w_1^{(2)}, w_2^{(2)}$.